

Stellar Masses and Star-Formation Rates of Galaxies and AGNs in the eFEDS GAMA09 Field

ZHIBO YU (喻知博) ^{1,2}, FAN ZOU (邹凡) ^{1,2} AND WILLIAM N. BRANDT ^{1,2,3}

¹*Department of Astronomy and Astrophysics, 525 Davey Lab, The Pennsylvania State University, University Park, PA 16802, USA*

²*Institute for Gravitation and the Cosmos, The Pennsylvania State University, University Park, PA 16802, USA*

³*Department of Physics, 104 Davey Laboratory, The Pennsylvania State University, University Park, PA 16802, USA*

ABSTRACT

The eFEDS is a wide ≈ 140 deg² field that has extensive multiwavelength coverage. To improve the utility of the existing data, we use CIGALE to fit source Spectral Energy Distributions (SEDs) from X-rays to far-infrared (FIR) mainly to derive stellar masses (M_*) and star-formation rates (SFRs) for normal galaxies and X-ray Active Galactic Nuclei (AGNs). The catalog consists of 2,057,027 galaxies and 10,373 X-ray AGNs located in the ≈ 60 deg² GAMA09 sub-field. Comparing our M_* with other available catalogs and our SFRs with FIR-derived SFRs, we demonstrate the general reliability of our SED-fitting measurements. Our catalog is publicly available at [10.5281/zenodo.10127224](https://doi.org/10.5281/zenodo.10127224).

1. INTRODUCTION

The eROSITA Final Equatorial Depth Survey (eFEDS) was the largest observational investment during the eROSITA performance verification phase. The entire field, spanning ≈ 140 deg², was observed to a depth of ≈ 2.2 ks by eROSITA (Brunner et al. 2022; Salvato et al. 2022). eFEDS was constructed to encompass the ≈ 60 deg² GAMA09 field (Driver et al. 2022), which has rich multi-wavelength data. Given the X-ray coverage from eROSITA and the well-cataloged photometric data from UV to FIR on a 10²-deg² scale, eFEDS is useful for both AGN and galaxy studies. To facilitate future studies, we report M_* and SFRs for ≈ 2 million sources in the eFEDS GAMA09 field primarily utilizing the GAMA-derived photometric catalog that is based upon KiDS and VIKING imaging data (Bellstedt et al. 2020). The SED fitting was performed with CIGALE (Boquien et al. 2019; Yang et al. 2022).

2. DATA AND METHODS

Our analysis focuses on the GAMA09 region since the remaining parts of eFEDS lack sufficient multi-wavelength coverage, especially the NIR coverage provided by KiDS and VIKING, which are crucial in deriving reliable M_* . We select X-ray AGNs based on the eFEDS X-ray main catalog (Brunner et al. 2022), and the intrinsic X-ray fluxes are taken from Liu et al. (2022) who corrected for absorption via X-ray spectral analyses. The rest of the sources are classified as galaxies. The UV-to-FIR photometry is from the GAMA-KiDS-VIKING (GKV) catalog compiled in Bellstedt et al. (2020). In general, the multiwavelength coverage is uniform, reaching 5σ depths of 24.2 mag and 21.3 mag for i -band and K_S -band, respectively. We also incorporate the HSC-Wide survey to support the optical coverage, which uniformly covers the entire GAMA09 region with a 5σ limiting magnitude of 26.1 mag in i -band (Aihara et al. 2022). The effective filter response and zero-point calibration across different HSC bands are also corrected. Both the GKV and HSC-Wide catalogs have accounted for Galactic extinction. Additionally, we include *Herschel* FIR photometry from the HELP collaboration (Shirley et al. 2021). The photometric redshifts (photo-zs) and spectroscopic redshifts (spec-zs) are taken from the compilations of Salvato et al. (2022) and Driver et al. (2022) for X-ray AGNs and normal galaxies, respectively. The photo-zs generally have good quality with typical dispersions of a few percent and outlier fractions of less than 10%. We also drop sources near bright stars so that the impact on our overall photometry is minimal. Our final sample contains 2,057,027 normal galaxies and 10,373 X-ray AGNs (including 9,856 with primary counterparts and 517 with secondary counterparts based upon the identifications of Salvato et al. 2022).

We apply the same methods as in [Zou et al. \(2022\)](#) to derive the best-fit M_* and SFRs. Briefly, **CIGALE** assumes an energy balance principle and decomposes a SED into several user-defined components (including AGNs). For normal galaxies and X-ray AGNs, we use the dense-grid **CIGALE** parameter settings for normal galaxies and AGN candidates in [Zou et al. \(2022\)](#), respectively (see their Tables 4 and 5). We fit the near-UV (NUV) to FIR SEDs for galaxies and add X-ray photometry for AGNs. To account for systematic uncertainties, 0.05 mag error is added in quadrature for all bands from NUV to NIR.

3. RESULTS

To evaluate the reliability of our M_* measurements, we compare our M_* for normal galaxies with the results from the GAMA collaboration ($M_{*,\text{ref}}$) ([Taylor et al. 2011](#)), which only include bright sources with GAMA spectra. For X-ray AGNs, we refer to the M_* measurements from [Li et al. \(2023\)](#). The comparisons are shown in the top-left panel of [Figure 1](#) where $\Delta \log M_* = \log M_* - \log M_{*,\text{ref}}$. For 59,653 normal galaxies and 2,029 X-ray AGNs, $\sigma_{\text{NMAD}} = 0.12$ and 0.23 with median $\Delta \log M_* = 0.02$ and -0.12 , where σ_{NMAD} is the normalized median absolute deviation (NMAD).¹ To assess the SFR measurements, we compare SFRs based upon our SED-fitting and FIR-based SFRs (SFR_{FIR}) that are derived following the method in [Chen et al. \(2013\)](#). We also correct for old-star heating following Equation 25 in [Zou et al. \(2022\)](#). [Figure 1](#) top-right panel shows the comparisons between different SFRs for both galaxies and X-ray AGNs, where $\Delta \log \text{SFR} = \log \text{SFR} - \log \text{SFR}_{\text{FIR}}$. For 34,610 galaxies and 862 X-ray AGNs with FIR signal-to-noise ratio (SNR) > 5 , $\sigma_{\text{NMAD}} = 0.41$ and 0.28 with median $\Delta \log \text{SFR} = -0.19$ and 0.04, respectively. These values are generally as good as those in [Zou et al. \(2022\)](#) where they fit SEDs to three million sources in the $\approx 13.2 \text{ deg}^2$ XMM-SERVS fields. Due to the large area and shallow X-ray depth of eFEDS, there will be a significant fraction of BL AGNs whose AGN components generally dominate the NIR emission, causing less reliable M_* measurements. Thus, we also plot Broad-Line AGN (BL AGN) candidates in [Figure 1](#), which are selected as having AGN components constituting $> 50\%$ of the total flux density at rest-frame $1 \mu\text{m}$. The impact of a high AGN contribution on M_* is clearly shown by the widely scattered $\Delta \log M_*$ ($\sigma_{\text{NMAD}} = 0.66$). Apart from eFEDS, we also apply the same method for SED-fitting to COSMOS, and the results are consistent with the COSMOS2020 catalog by [Weaver et al. \(2022\)](#).

We further estimate the nominal depth of our measurements. We define “good bands” as those with SNR > 5 , and we plot the number of good bands vs. i -band magnitude in [Figure 1](#) bottom panel. The plot indicates that the SED quality in eFEDS degrades at i -mag ≈ 21.5 . Approximately 30% of our sources are brighter than this magnitude. Among these, 10% of normal galaxies and 43% of X-ray AGNs have available spec-zs. We only show sources with i -mag < 22 in [Figure 1](#) top panels, which constitute $\gtrsim 90\%$ of the sources that we compared. We warn readers to use our catalog at i -mag $\gtrsim 22$ cautiously, as fainter sources normally contain only ~ 6 bands primarily from HSC, and it is harder to constrain their properties due to lack of NIR coverage.

Our catalog is available at [10.5281/zenodo.10127224](https://doi.org/10.5281/zenodo.10127224). We provide the source M_* , SFRs, classifications (X-ray AGNs vs. normal galaxies), and necessary information that can be helpful to cross-reference GAMA objects and/or eFEDS X-ray/optical-IR counterparts. We also provide AGN fractional contributions at rest-frame 5000 \AA , $1 \mu\text{m}$, and integrated $8 - 1000 \mu\text{m}$ for X-ray AGNs to help readers identify sources with less-reliable M_* . Readers should also note that our AGN selection is based upon X-ray detection only, which is generally a good tracer of black-hole accretion rates (BHAR), but this selection is incomplete. To reach better completeness, one should combine multiple selection methods such as mid-infrared (MIR; e.g., [Zou et al. 2022](#)) and radio (e.g., [Zhu et al. 2023](#)).

Acknowledgments

We acknowledge support from NSF grant AST-2106990 and Penn State.

¹ NMAD is defined as $1.4826 \times$ median absolute deviation.

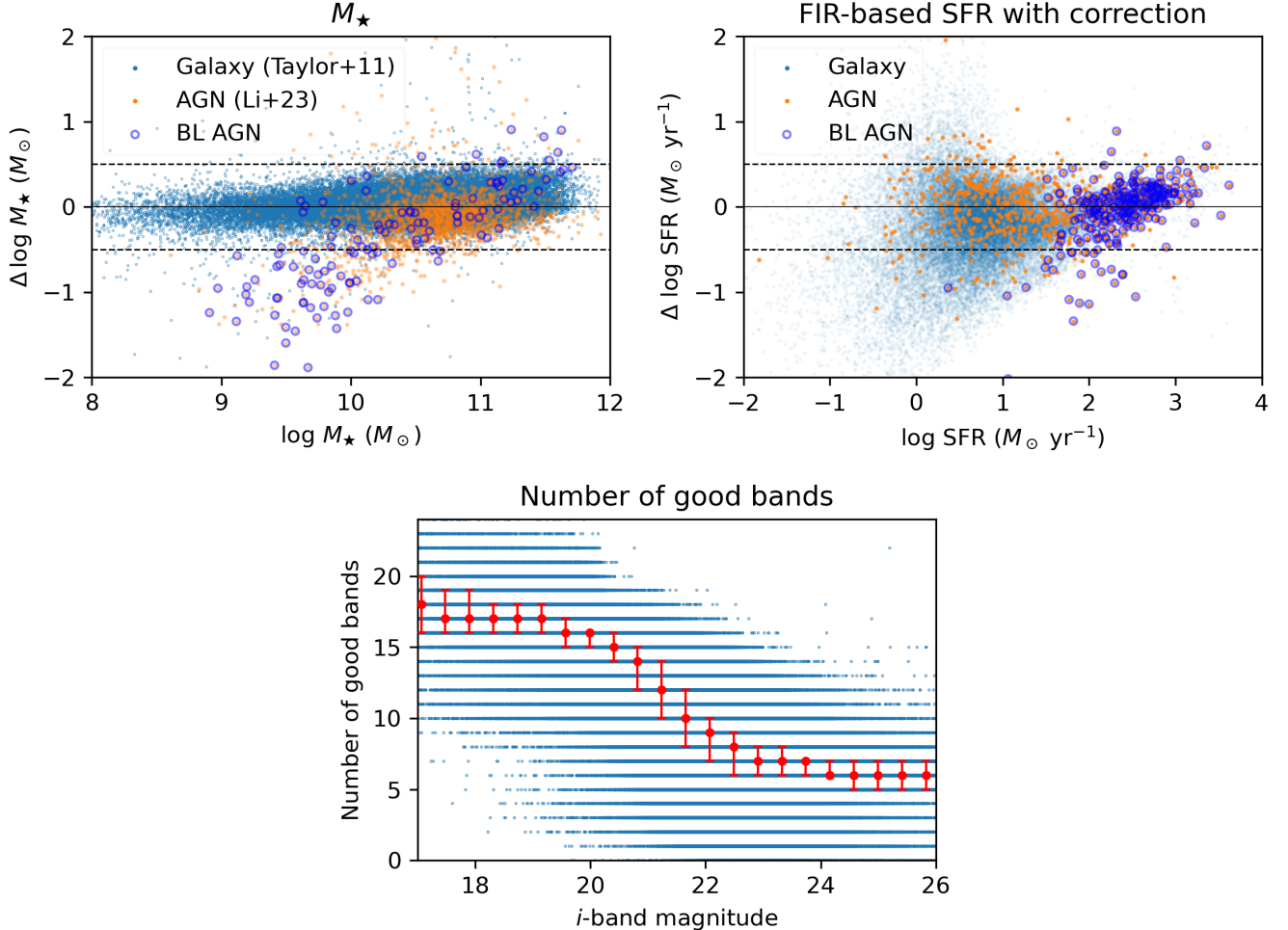


Figure 1. Top-left: Comparison between our M_\star and M_\star from existing catalogs in eFEDS. Top-right: Comparison between our SED-based SFRs and FIR-based SFRs. The dashed lines indicate 0.5 dex deviations. Note that we only plot sources with i -mag < 22 . Bottom: Number of good bands (with SNR > 5) vs. i -mag. Each blue point represents a source, and the red error bars represent the median, 25th, and 75th percentile of the number of good bands in each magnitude bin.

APPENDIX

A. SEDS IN COSMOS

The COSMOS field is one of the LSST Deep Drilling Fields (DDFs) and has been well characterized by many past studies (e.g., Marchesi et al. 2016; Weaver et al. 2022). Our purpose in working on COSMOS is to consistently measure the galaxy properties via SED-fitting in the same manner as for other DDFs (e.g., Zou et al. 2022). In this work, our methods for COSMOS are the same as those for eFEDS and Zou et al. (2022). We focus on the 1.27 deg^2 UltraVISTA footprint inside COSMOS because sufficiently deep NIR coverage is critical in deriving reliable M_\star . The final catalog consists of 709,087 normal galaxies and 2,209 X-ray AGNs. The absorption-corrected X-ray data are from Civano et al. (2016) and Marchesi et al. (2016). The UV-to-MIR data are from *the Farmer* catalog in the COSMOS2020 data release (Weaver et al. 2022). To optimize the magnitude offsets in each band, we apply the correction in Table 3 of Weaver et al. (2022). We also add the $24\text{--}500 \mu\text{m}$ data from the “super-deblended” FIR photometric catalog in Jin et al. (2018). The Galactic extinction is corrected following the methods in Section 2.6 of Zou et al. (2022). The

redshifts for X-ray AGNs and normal galaxies are from [Marchesi et al. \(2016\)](#) and [Weaver et al. \(2022\)](#), respectively. The quality of the photo-zs is generally good, with typical dispersions of 1–4% and outlier fractions of a few percent.

We compare our M_* with other measurements in the top-left panel of Figure 2. The M_* values for 703,081 galaxies are compared with those in *the Farmer* catalog. The median $\Delta \log M_* = 0.07$, and $\sigma_{\text{NMAD}} = 0.15$. We compare 2,086 X-ray AGNs with those in [Zou et al. \(2019\)](#), who also include AGN components when deriving M_* . The median $\Delta \log M_* = 0.09$, and $\sigma_{\text{NMAD}} = 0.21$. We also select BL AGN candidates with AGN components contributing $> 50\%$ of the total flux density at rest-frame $1 \mu\text{m}$. The result indicates this criterion is efficient in selecting AGNs with problematic M_* measurements as almost all sources with $\Delta \log M_* < -0.5$ are selected. The impact of these BL AGN candidates on COSMOS should be much reduced compared to eFEDS because of the small area and greater depth of COSMOS. This is supported by the much-reduced fraction of sources with AGN contribution at rest-frame $1 \mu\text{m} > 50\%$ in COSMOS (9%) than in eFEDS (32%). In addition, among our X-ray AGNs, 36 are spectroscopically confirmed BL AGNs by [Suh et al. \(2020\)](#). The median $\Delta \log M_*$ is -0.40 , which is consistent with the findings in [Zhuang et al. \(2023\)](#). In Figure 2 top-right panel, we compare SED-based SFRs and FIR-based SFRs corrected for old-star heating. For 4,017 galaxies and 225 AGNs with FIR SNR > 5 , $\sigma_{\text{NMAD}} = 0.23$ and 0.27 with median $\Delta \log \text{SFR} = -0.06$ and 0.05 , respectively. Our measurements in COSMOS are generally consistent with the previous results.

The nominal depth in COSMOS is also shown in the bottom panel of Figure 2. The number of good bands in COSMOS is much larger than that in eFEDS at the bright end, but it dramatically degrades at $i\text{-mag} \approx 25.5$. Approximately 35% of our sources are brighter than this magnitude. Among these, 64% of X-ray AGNs have spec-zs from [Marchesi et al. \(2016\)](#).² In the Figure 2 top panels, we only show sources with $i\text{-mag} < 26$. We warn readers to use our catalog at $i\text{-mag} \gtrsim 26$ cautiously as fainter sources generally have only a handful of bands, so the SED fitting becomes unreliable.

² The spec-zs for normal galaxies in the COSMOS2020 data release are not publicly available, so we only adopt their photo-zs. Since their photo-zs agree well with the spec-zs, the adoption of photo-zs should not materially affect our conclusions.

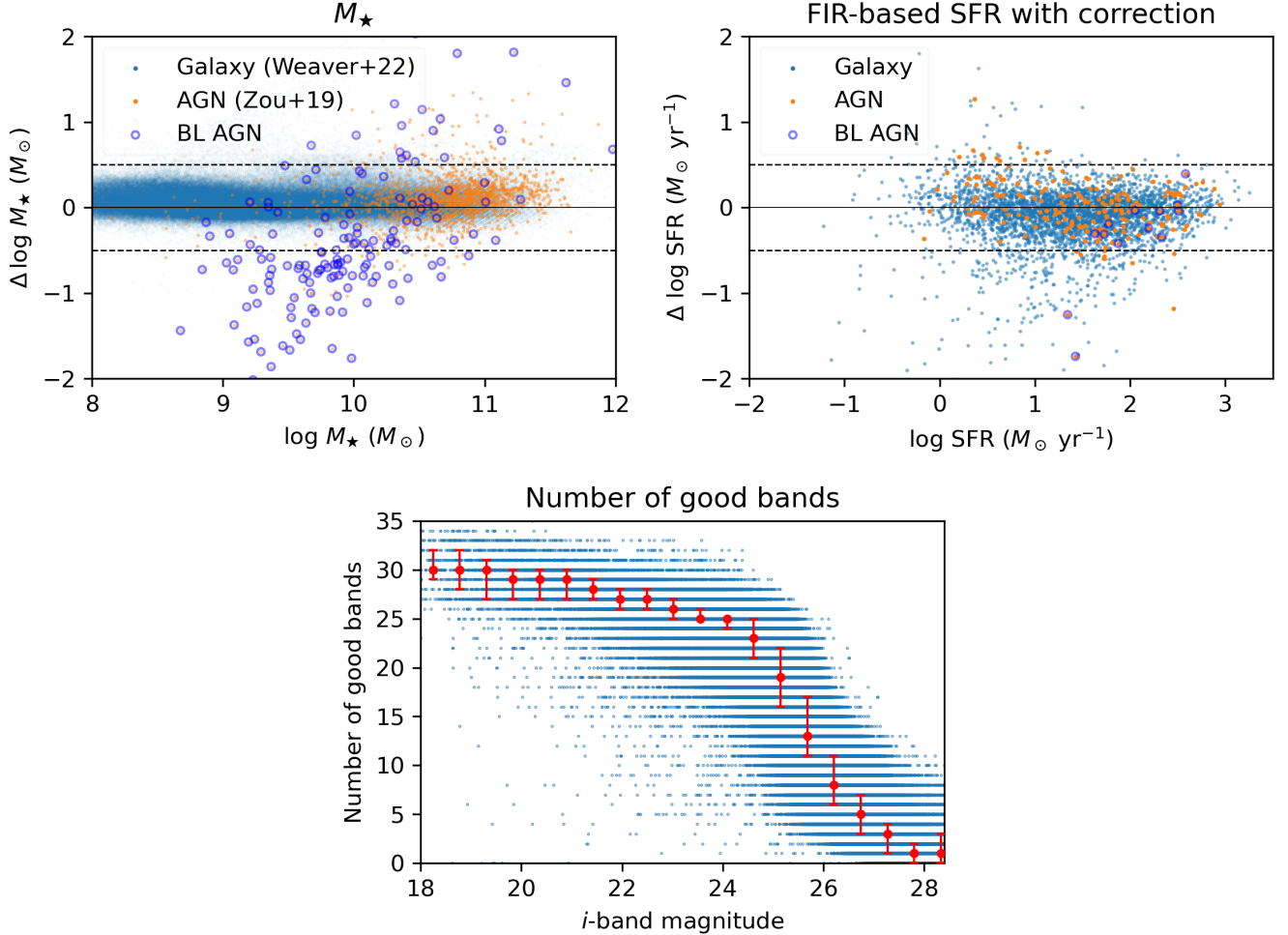


Figure 2. Top-left: Comparison between our M_{\star} and M_{\star} from existing catalogs in COSMOS. Top-right: Comparison between our SED-based SFRs and FIR-based SFRs. The dashed lines indicate 0.5 dex deviations. Note that we only plot sources with i -mag < 26 . Bottom: Number of good bands (with SNR > 5) vs. i -mag. Each blue point represents a source, and the red error bars represent the median, 25th, and 75th percentile of the number of good bands in each magnitude bin.

REFERENCES

- Aihara, H., AlSayyad, Y., Ando, M., et al. 2022, PASJ, 74, 247, doi: [10.1093/pasj/psab122](https://doi.org/10.1093/pasj/psab122)
- Bellstedt, S., Driver, S. P., Robotham, A. S. G., et al. 2020, MNRAS, 496, 3235, doi: [10.1093/mnras/staa1466](https://doi.org/10.1093/mnras/staa1466)
- Boquien, M., Burgarella, D., Roehlly, Y., et al. 2019, A&A, 622, A103, doi: [10.1051/0004-6361/201834156](https://doi.org/10.1051/0004-6361/201834156)
- Brunner, H., Liu, T., Lamer, G., et al. 2022, A&A, 661, A1, doi: [10.1051/0004-6361/202141266](https://doi.org/10.1051/0004-6361/202141266)
- Chen, C.-T. J., Hickox, R. C., Alberts, S., et al. 2013, ApJ, 773, 3, doi: [10.1088/0004-637X/773/1/3](https://doi.org/10.1088/0004-637X/773/1/3)
- Civano, F., Marchesi, S., Comastri, A., et al. 2016, ApJ, 819, 62, doi: [10.3847/0004-637X/819/1/62](https://doi.org/10.3847/0004-637X/819/1/62)
- Driver, S. P., Bellstedt, S., Robotham, A. S. G., et al. 2022, MNRAS, 513, 439, doi: [10.1093/mnras/stac472](https://doi.org/10.1093/mnras/stac472)
- Jin, S., Daddi, E., Liu, D., et al. 2018, ApJ, 864, 56, doi: [10.3847/1538-4357/aad4af](https://doi.org/10.3847/1538-4357/aad4af)
- Li, J., Silverman, J. D., Merloni, A., et al. 2023, arXiv e-prints, arXiv:2302.12438, doi: [10.48550/arXiv.2302.12438](https://doi.org/10.48550/arXiv.2302.12438)
- Liu, T., Buchner, J., Nandra, K., et al. 2022, A&A, 661, A5, doi: [10.1051/0004-6361/202141643](https://doi.org/10.1051/0004-6361/202141643)
- Marchesi, S., Civano, F., Elvis, M., et al. 2016, ApJ, 817, 34, doi: [10.3847/0004-637X/817/1/34](https://doi.org/10.3847/0004-637X/817/1/34)
- Salvato, M., Wolf, J., Dwelly, T., et al. 2022, A&A, 661, A3, doi: [10.1051/0004-6361/202141631](https://doi.org/10.1051/0004-6361/202141631)
- Shirley, R., Duncan, K., Campos Varillas, M. C., et al. 2021, MNRAS, 507, 129, doi: [10.1093/mnras/stab1526](https://doi.org/10.1093/mnras/stab1526)

- Suh, H., Civano, F., Trakhtenbrot, B., et al. 2020, ApJ, 889, 32, doi: [10.3847/1538-4357/ab5f5f](https://doi.org/10.3847/1538-4357/ab5f5f)
- Taylor, E. N., Hopkins, A. M., Baldry, I. K., et al. 2011, MNRAS, 418, 1587, doi: [10.1111/j.1365-2966.2011.19536.x](https://doi.org/10.1111/j.1365-2966.2011.19536.x)
- Weaver, J. R., Kauffmann, O. B., Ilbert, O., et al. 2022, ApJS, 258, 11, doi: [10.3847/1538-4365/ac3078](https://doi.org/10.3847/1538-4365/ac3078)
- Yang, G., Boquien, M., Brandt, W. N., et al. 2022, ApJ, 927, 192, doi: [10.3847/1538-4357/ac4971](https://doi.org/10.3847/1538-4357/ac4971)
- Zhu, S., Brandt, W. N., Zou, F., et al. 2023, MNRAS, 522, 3506, doi: [10.1093/mnras/stad1178](https://doi.org/10.1093/mnras/stad1178)
- Zhuang, M.-Y., Li, J., & Shen, Y. 2023, arXiv e-prints, arXiv:2309.03266, doi: [10.48550/arXiv.2309.03266](https://doi.org/10.48550/arXiv.2309.03266)
- Zou, F., Yang, G., Brandt, W. N., & Xue, Y. 2019, ApJ, 878, 11, doi: [10.3847/1538-4357/ab1eb1](https://doi.org/10.3847/1538-4357/ab1eb1)
- Zou, F., Brandt, W. N., Chen, C.-T., et al. 2022, ApJS, 262, 15, doi: [10.3847/1538-4365/ac7bdf](https://doi.org/10.3847/1538-4365/ac7bdf)